metals

Article

Reducing the Eddy Current Losses in Nd–Fe–B Magnets Through Si Addition

Tetsuji Saito [1,*] and Daisuke Nishio-Hamane [2]

[1] Graduate School of Engineering, Chiba Institute of Technology, Narashino 275-8588, Japan
[2] Institute for Solid State Physics, The University of Tokyo, Kashiwa 277-8581, Japan; hamane@issp.u-tokyo.ac.jp
* Correspondence: tetsuji.saito@it-chiba.ac.jp

Abstract

Electric motors that use neodymium–iron–boron (Nd–Fe–B) magnets are at the forefront of global efforts to reduce greenhouse gas emissions. However, a major problem associated with these motors is thermal demagnetization driven by eddy current (EC) losses in the magnets; the relatively low electrical resistivity of Nd–Fe–B magnets means that the magnetic fields in the motor generate considerable EC losses. In this study, Nd–Fe–B magnets with 0–20 wt% Si additives were produced through hot pressing to investigate the effects of Si addition on magnetic properties and electrical resistivity. Small amounts of Si significantly increased electrical resistivity without negatively affecting the magnetic properties. The high coercivity of the Nd–Fe–B magnets, 12.5 kOe, did not decrease even in the presence of up to 15 wt% Si content. The electrical resistivity of Nd–Fe–B magnets increased monotonically as the Si content increased, from 1.43 μΩm for pure Nd–Fe–B magnets to 8.17 μΩm with 20% Si. As the electrical resistivity increased, the associated EC losses decreased; the estimated EC losses were halved with the addition of ~8 wt% Si, and further decreased to one-third through the addition of ~12 wt% Si, while simultaneously maintaining high coercivity.

Keywords: Nd–Fe–B magnet; magnetic property; electrical resistivity; eddy current loss

1. Introduction

Clean, renewable energy is critical to achieving the United Nations Sustainable Development Goals. Furthermore, carbon neutrality—defined as reducing net greenhouse gas (such as CO_2) emissions to zero—has become a global priority, with many countries aiming to achieve full decarbonization by 2050 [1]. Technologies that harness renewable energy sources, including solar panels, wind turbines, and environmentally friendly vehicles, have been widely adopted to reduce emissions [2]. In wind turbines, generators convert mechanical energy into electrical energy. In hybrid or electric vehicles, motors efficiently convert electrical energy into mechanical energy. The generators and motors driving these technologies require high-performance permanent magnets [3,4], with neodymium–iron–boron (Nd–Fe–B) magnets, which contain the rare earth metal neodymium, commonly used. Such Nd–Fe–B magnets have widespread industrial applications in highly efficient motors and cane also be found in voice coil motors for hard disk drives. With expanding efforts to mitigate climate change, the demand for Nd–Fe–B magnets is expected to increase significantly in the near future [5–7].

Check for updates

Academic Editor: Imre Bakonyi

Received: 20 April 2026
Revised: 20 May 2026
Accepted: 20 May 2026
Published: 22 May 2026

Copyright: © 2026 by the authors. Licensee MDPI, Basel, Switzerland. This article is an open access article distributed under the terms and conditions of the Creative Commons Attribution (CC BY) license.

However, in motors, changing the magnetic field can induce eddy currents (ECs) in the permanent magnet [8–16]. As Nd–Fe–B magnets are essentially metallic with low resistivity, considerable EC losses can result from magnetic field changes in the motor. EC losses heat the magnets, inducing thermal demagnetization and reducing their coercivity. It is thus essential to minimize the EC losses of Nd–Fe–B magnets used in motors. In practice, two methods can be employed to mitigate the thermal reduction in coercivity in Nd–Fe–B magnets: (i) increasing coercivity and (ii) reducing EC losses.

The current standard approach involves sufficiently increasing the baseline coercivity of the Nd–Fe–B magnet to sufficiently maintain the required coercivity at the elevated temperatures resulting from EC losses. The conventional method involves heavy rare earth metals, such as Dy or Tb; the coercivities of the $Dy_2Fe_{14}B$ and $Tb_2Fe_{14}B$ phases are much higher than that of the $Nd_2Fe_{14}B$ phase in Nd–Fe–B magnets [17–19]. The resultant Nd–Dy–Fe–B and Nd–Tb–Fe–B magnets with $(Nd,Dy)_2Fe_{14}B$ and $(Nd,Tb)_2Fe_{14}B$ phases exhibit extremely large coercivities.

The main problems associated with heavy rare earth additions are their high cost and the reduced maximum energy products $(BH)_{max}$. Accordingly, considerable effort has been devoted to reducing the amount of heavy rare earth additions [20–22]. The grain-boundary diffusion process (GBDP) is a key technology for Nd–Fe–B magnets, significantly improving coercivity while minimizing the need for heavy rare earths. In the GBDP, the heavy rare-earth elements diffuse and dissolve only at the surface of the Nd2Fe14B phase, forming $(Nd,Dy)_2Fe_{14}B$ and $(Nd,Tb)_2Fe_{14}B$ surface phases with high coercivity, which effectively improve the overall coercivity of the magnet.

An alternative method to increase the coercivity of Nd–Fe–B magnets involves the addition of light rare earth eutectic alloys, such as Nd-Cu and Pr-Cu [23–26]. The GBDP for such eutectic alloys has been extensively investigated, demonstrating an effective increase in the coercivity of Nd–Fe–B magnets. Unlike heavy rare-earth additions, light rare-earth eutectic alloys diffuse into the grain-boundary phase, increasing the grain boundary phase thickness and reducing the intergranular exchange coupling between the Nd2Fe14B phases, thereby enhancing the overall coercivity of the Nd–Fe–B magnets.

The addition of heavy and light rare earth elements increases the room-temperature coercivities of Nd–Fe–B magnets, enabling their use at high temperatures resulting from EC losses in the magnet. However, the rare earth element additions also result in a decrease in the overall magnetization.

From the above evidence, it is thus preferable to reduce EC losses to mitigate the thermal reduction in coercivity. One method to reduce EC losses involves dividing the magnet into several insulated segments, thereby disrupting the ECs [27–30]. Accordingly, Nd–Fe–B magnets used in motors are often divided into multiple segments. Magnet segmentation is currently the preferred option as it does not require the magnet composition to be altered (i.e., there are no rare-earth additions).

Another effective method to reduce EC losses involves increasing the electrical resistivity of the magnets used, as EC losses are inversely proportional to the electrical resistivity. Thus, enhancing the electrical resistivity of the magnet effectively suppresses EC losses without requiring complex magnet segmentation. However, increasing the electrical resistivity of Nd–Fe–B magnets is challenging due to their fundamental material properties and requires additions to the material composition. Efforts have been made to increase the electrical resistivity of Nd–Fe–B magnets using additives such as NaF_3 or CaF_2 [31–33]. However, the large quantities of nonmagnetic additives required lead to significant deterioration in magnetic properties. In other studies, the addition of DyF_3 or DyN increased the electrical resistivity of Nd–Fe–B magnets without reducing coercivity; however, this approach requires the use of the undesirable heavy rare earth element Dy [34–39].

Accordingly, achieving simultaneous improvements in coercivity and electrical resistivity in Nd–Fe–B magnets for motor applications without the rare earth additions would be highly advantageous. Herein, we demonstrate that the addition of small amounts of Si significantly increases the electrical resistivity without deteriorating the magnetic properties of Nd–Fe–B magnets prepared through hot pressing. The structures and magnetic properties of Nd–Fe–B magnets with Si additions are discussed below.

2. Materials and Methods

Commercial Nd–Fe–B melt-spin ribbons (MQ powder; Magnequench, Pendleton, IN, USA) were used as the starting powder. The MQ powder was thoroughly blended with Si powder (0–20 wt%) using a mortar and pestle. Next, 2 g of blended powder was placed in a boron nitride-coated carbon die and positioned in the spark plasma sintering equipment (SPS; S. S. Alloy, Hiroshima, Japan). The powder was hot-pressed under vacuum using SPS equipment; the powder was heated from room temperature to 873 K over 300 s, held at 873 K for 300 s under a uniaxial pressure of 50 MPa, and then slowly cooled to room temperature. The cooled hot-pressed magnets were extracted from the SPS equipment and removed from the carbon die.

After the densities of the hot-pressed specimens were measured by the Archimedes method with a semi-micro analytical balance (AND, GR-120, Tokyo, Japan)), the crystal structures of the hot-pressed magnets were examined via X-ray diffraction (XRD; Rigaku MiniFlex600, Tokyo, Japan) using Cu K_α radiation. The microstructures of the hot-pressed magnets were imaged using a scanning electron microscope (SEM; JEOL, JEM IT-100, Tokyo, Japan). Needle-like ($1 \times 1 \times 8$ mm) and rod-like specimens ($2 \times 2 \times 7$ mm) were cut from hot-pressed magnets using a low-speed diamond saw. The hysteresis loops of needle-like specimens—chosen to avoid demagnetization correction—were measured at room temperature with a vibrating sample magnetometer (VSM; Riken Denshi BHV-525RSCM, Tokyo, Japan) after premagnetization in a pulsed field of 50 kOe. Several specimens were measured to ensure the reliability of the coercivity value. The electrical properties of rod-like specimens were measured using the four-probe method (Advance Riko, ZEM-3, Kanagawa, Japan).

3. Results

The Nd–Fe–B melt-spun ribbons were successfully hot-pressed to form Nd–Fe–B magnets with and without the addition of Si powder. The Nd–Fe–B magnets had a relatively high density of around 98%. The XRD patterns of the Nd–Fe–B magnets are shown in Figure 1. The XRD pattern of the Nd–Fe–B magnet is consistent with the hard-magnetic $Nd_2Fe_{14}B$ phase, with no noticeable diffraction peaks from any other phase. The addition of 5 wt% Si introduced clear diffraction peaks of the Si phase, combined with those of the $Nd_2Fe_{14}B$ phase. The diffraction peaks of the $Nd_2Fe_{14}B$ phase become less intense, and those of the Si phase become more intense as the Si content increases. The XRD results confirm that the hot-pressed Nd–Fe–B magnet with 5–20 wt% Si consisted of the $Nd_2Fe_{14}B$ and Si phases.

The microstructures of the hot-pressed Nd–Fe–B magnets are shown in Figure 2. The microstructure of the pure Nd–Fe–B magnet shows the layered structures of the melt-spun ribbons, outlined by particle boundaries (seen as thin white lines), where the ribbon surface melted and solidified during hot-pressing. Only a few small voids (seen as black dots) are found in the microstructure. These observations confirm that the Nd–Fe–B melt-spun ribbons are consolidated well into the Nd–Fe–B magnets. With the addition of Si, the melt-spun ribbons (light gray regions) and Si powders (dark gray regions) can be clearly observed. In Si-rich (15–20% Si) specimens' microstructures, black voids—formed during

specimen preparation for SEM studies—are also present. Together, these observations indicate that the Nd–Fe–B melt-spun ribbons and Si powders do not react with each other at this sintering temperature.

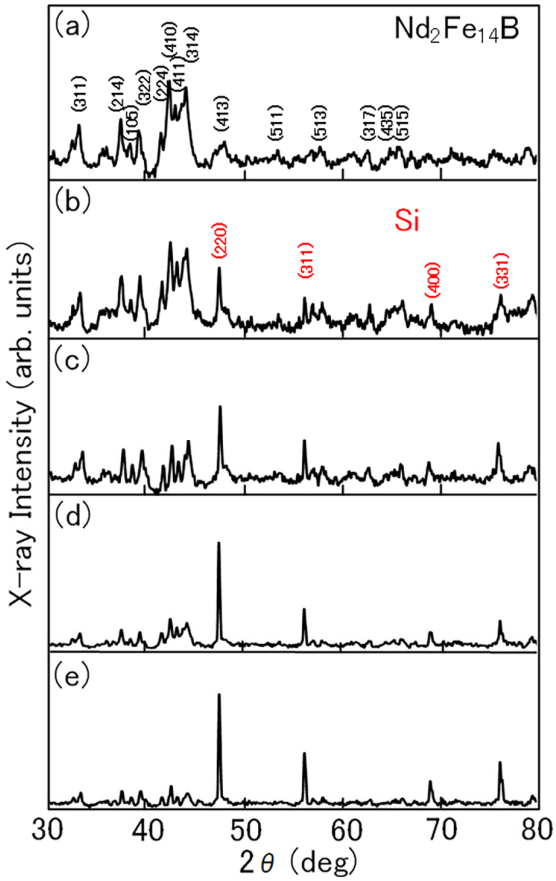

Figure 1. XRD patterns of the Nd–Fe–B magnets: (**a**) Nd–Fe–B, (**b**) 5 wt% Si, (**c**) 10 wt% Si, (**d**) 15 wt% Si, and (**e**) 20 wt% Si.

The influence of Si powder addition on the magnetic and electrical properties of the Nd–Fe–B magnets was examined. First, the magnetic properties were examined using VSM; the obtained hysteresis loops are shown in Figure 3. The applied magnetic field of 25 kOe is significantly lower than the field required to fully saturate the specimens, such that the hysteresis loop is classified as a minor loop. The pure Nd–Fe–B magnets exhibited a wide hysteresis loop with a high coercivity, attributed to the presence of the hard-magnetic $Nd_2Fe_{14}B$ phase. The addition of up to 15 wt% Si did not change the shape of the hysteresis loops; rather, an increase in the squareness of the hysteresis loops was noted with 5–15 wt% Si. However, further increases in Si content resulted in a contraction of the hysteresis loop. The overall VSM results indicated that the addition of up to 15 wt% Si did not significantly degrade the magnetic properties of the Nd–Fe–B magnets.

The saturation magnetization (i.e., magnetization in a maximal field of 25 kOe) and coercivities of the Nd–Fe–B magnets obtained from the hysteresis loops are summarized in Figure 4. The nonmagnetic Si powder caused the saturation magnetization of the Nd–Fe–B magnets to decrease gradually as the Si content increased, from 105 emu/g for the pure Nd–Fe–B magnet to 82 emu/g with 20 wt% Si. In contrast, the coercivity remained unchanged (or slightly increased) up to 15 wt% Si but decreased with further increases in Si content.

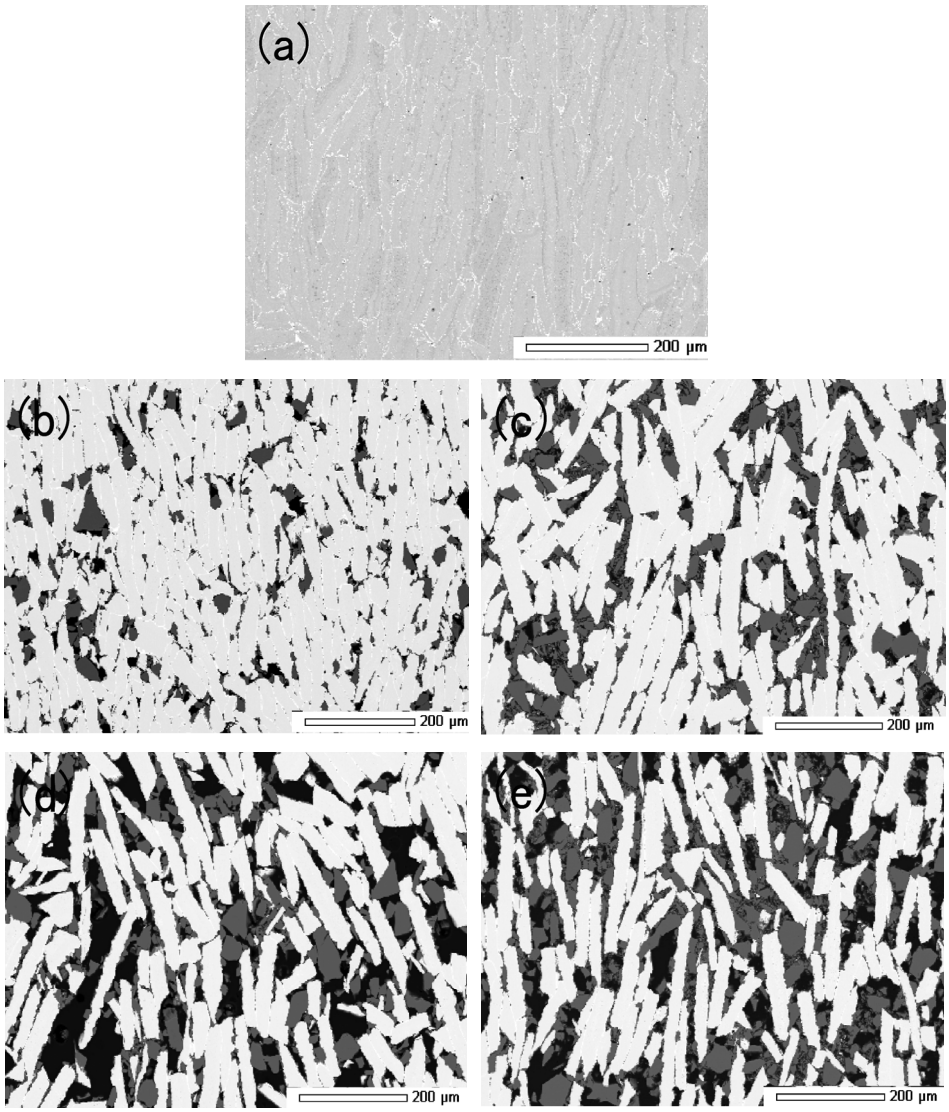

Figure 2. SEM images of the Nd–Fe–B magnets: (**a**) Nd–Fe–B, (**b**) 5 wt% Si, (**c**) 10 wt% Si, (**d**) 15 wt% Si, and (**e**) 20 wt% Si.

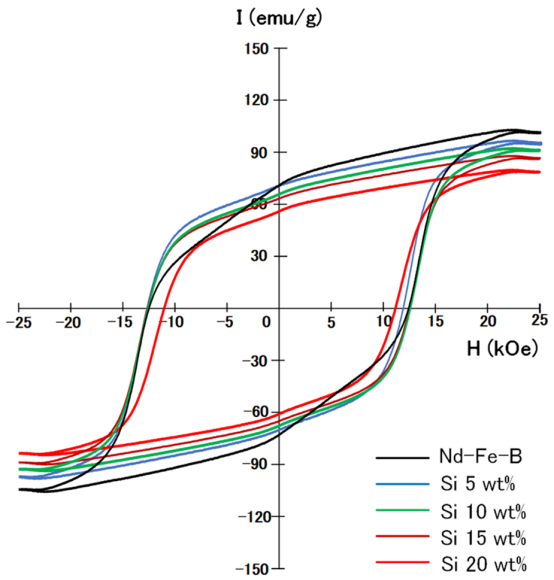

Figure 3. Hysteresis loops of the Nd–Fe–B magnets with different amounts of Si content.

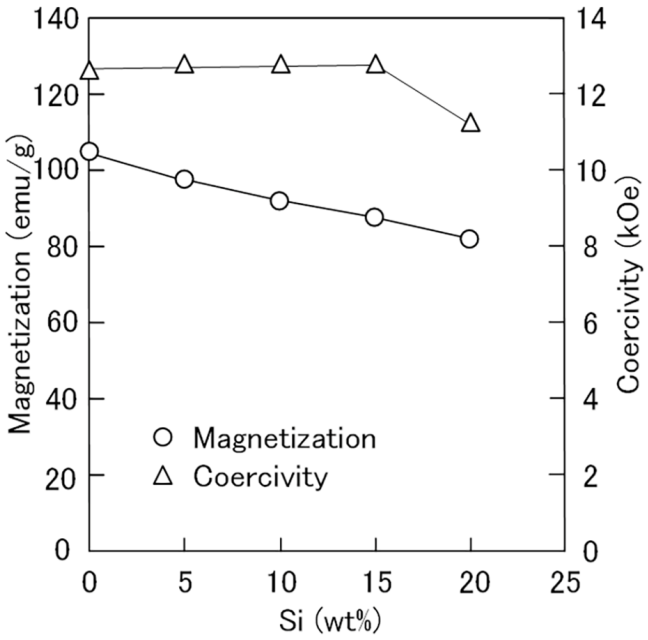

Figure 4. Dependence of the saturation magnetization (i.e., magnetization in a maximal field of 25 kOe) and coercivity of the Nd–Fe–B magnets on Si content.

The electrical resistivity of the Nd–Fe–B magnets was examined using the four-probe method; the results are shown in Figure 5. The electrical resistivity of the pure Nd–Fe–B magnets was 1.43 μΩm, comparable to that of the Nd–Fe–B melt-spun ribbons and sintered magnets in prior studies [40,41]. The high electrical resistivity (>1 kΩm) of the Si powder drove a monotonic increase in the overall electrical resistivity as the Si content increased, reaching 8.17 μΩm with 20 wt% Si. These results confirmed that the electrical resistivity of Nd–Fe–B magnets can be increased by the addition of Si.

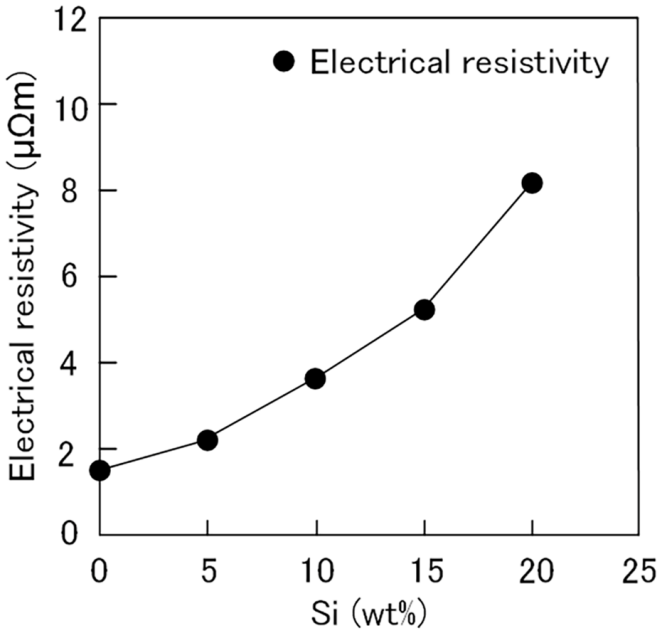

Figure 5. Dependence of the electrical resistivity of the Nd–Fe–B magnets on Si content.

4. Discussion

In this study, it has been demonstrated that the electrical resistivity of Nd–Fe–B magnets can be increased without reducing their coercivity through Si addition. The calculated variation in the electrical resistivity and coercivity for different Si content is shown in Figure 6 (the electrical resistivity and coercivity of the pure Nd–Fe–B magnets are set as the 100% baseline). The electrical resistivity increased markedly with increasing Si content, doubling at ~8 wt% Si, tripling at ~12 wt% Si, and reaching 567% at 20 wt% Si. This finding demonstrated that the addition of Si to Nd–Fe–B magnets was highly effective in increasing their electrical resistivity. Moreover, the addition of up to 15 we% Si did not degrade the coercivity. Together, these results confirmed that Si addition significantly increased electrical resistivity without inducing unwanted decreases in coercivity.

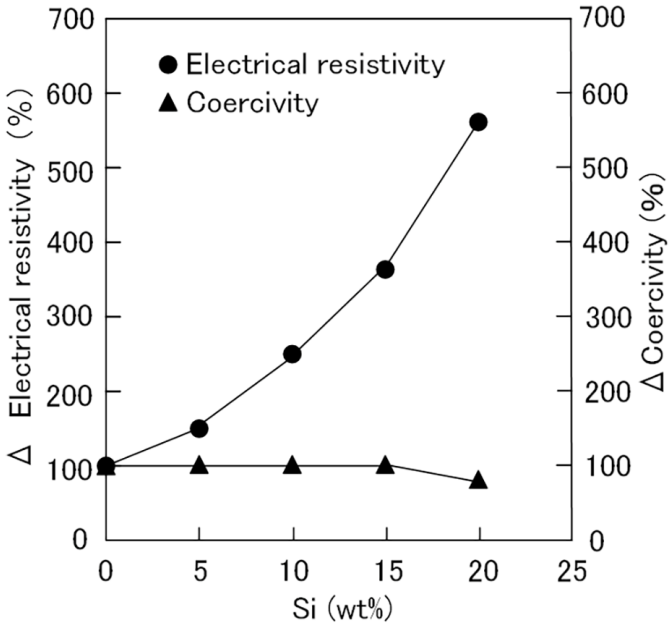

Figure 6. Variation in the electrical resistivity and coercivity of the Nd–Fe–B magnets with different Si content (normalized to the electrical resistivity and coercivity of Nd–Fe–B magnets at 100%).

EC losses, induced by the alternating fields, occur due to electrical resistance within the magnet core. The EC losses, P, can be expressed as follows [42]:

$$P = CB^2f^2d^2/\rho$$

where C is a proportionality constant, B is the flux density, f is the frequency, d is the thickness of the material, and ρ is the electrical resistivity. P is inversely proportional to ρ; thus, the most effective approach to reduce EC losses is to increase ρ. In this study, ρ was increased through the addition of Si to the Nd–Fe–B magnets. Figure 7 illustrates the estimated EC losses due to the obtained variation in ρ, with P decreasing significantly with increasing Si content—the EC losses were halved by the addition of ~8 wt% Si and reduced to 1/3 by the addition of ~12 wt% Si. However, the addition of nonmagnetic Si to Nd–Fe–B magnets decreases the magnetization (i.e., the flux density B), such that the actual EC losses of the Nd–Fe–B magnets become smaller than the estimated EC losses presented in Figure 7. It has been suggested that the thermal demagnetization of Nd–Fe–B magnets, particularly the reduction in coercivity, is due to heating from EC losses. Herein, it has been shown that Si addition can reduce the EC losses of Nd–Fe–B magnets by 1/3 without degrading their coercivity.

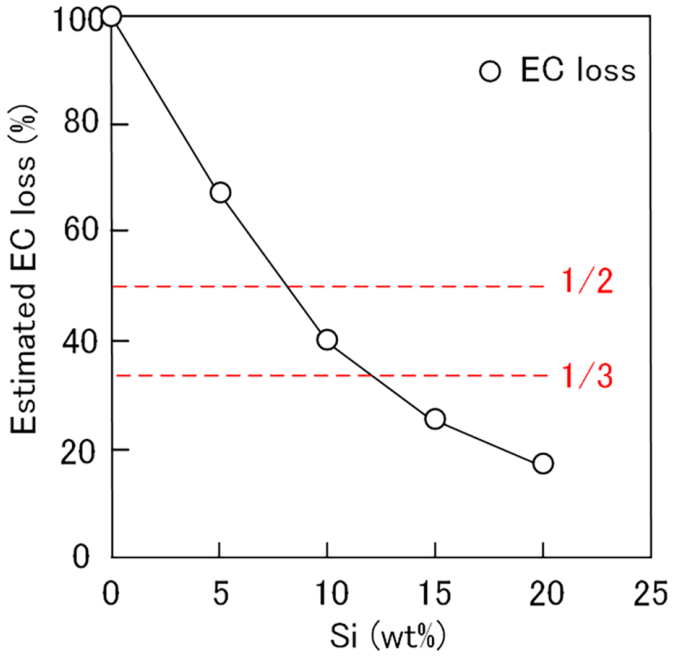

Figure 7. Variation in the estimated EC loss of the Nd–Fe–B magnets with different Si content (normalized to the electrical resistivity and coercivity of Nd–Fe–B magnets at 100%).

5. Conclusions

In this study, Nd–Fe–B magnets with 0–20 wt% Si were produced from commercial Nd–Fe–B melt-spin ribbons through hot pressing to investigate the effects of Si content on electrical resistivity. The Nd–Fe–B magnet consisted of a hard-magnetic $Nd_2Fe_{14}B$ phase, whereas the Nd–Fe–B magnets with 5–20 wt% Si powders consisted of the hard-magnetic $Nd_2Fe_{14}B$ phase combined with a nonmagnetic Si phase. The Nd–Fe–B magnets exhibited a high coercivity of 12.5 kOe and a high saturation magnetization of 105 emu/g. The saturation magnetization of the Nd–Fe–B magnets gradually decreased with increasing nonmagnetic Si content. In contrast, the coercivity of the Nd–Fe–B magnets did not decrease in the presence of Si up to a content of 15 wt% (although 20 wt% Si resulted in lower coercivity and saturation magnetization). The Nd–Fe–B magnets possessed an electrical resistivity of 1.43 μΩm, which monotonically increased with increasing Si content due to the higher electrical resistivity of Si. The increase in electrical resistivity of the Nd–Fe–B magnets halved the EC losses when adding ~8 wt% Si, and adding ~12 wt% Si reduced them by 1/3, while simultaneously retaining high coercivity.

Author Contributions: Conceptualization, T.S.; methodology, T.S.; formal analysis, T.S. and D.N.-H.; investigation, T.S. and D.N.-H.; resources, T.S.; data curation, T.S. and D.N.-H.; writing—original draft preparation, T.S.; funding acquisition, T.S. All authors have read and agreed to the published version of the manuscript.

Funding: This work was supported by a Grant-in-Aid from the Tsugawa Foundation, entitled “The research of rare-earth magnets with high electrical resistivity for motor application”.

Data Availability Statement: The raw data supporting the conclusions of this article will be made available by the authors on request.

Acknowledgments: This work was performed using the facilities of the Institute for Solid State Physics, the University of Tokyo.

Conflicts of Interest: The authors declare no conflicts of interest.

References

1. Zhang, S.; Cai, W.; Zheng, X.; Lv, X.; An, K.; Cao, Y.; Cheng, H.S.; Dai, J.; Dong, X.; Fan, S.; et al. Global readiness for carbon neutrality: From targets to action. *Environ. Sci. Ecotechnol.* **2025**, *25*, 100546. [CrossRef] [PubMed]
2. Shang, Y.; Sang, S.; Tiwari, A.K.; Khan, S.; Zhao, X. Impacts of renewable energy on climate risk: A global perspective for energy transition in a climate adaptation framework. *Appl. Energy* **2024**, *362*, 122994. [CrossRef]
3. Ghorbani, Y.; Ilankoon, I.M.S.K.; Dushyantha, N.; Nwaila, G.T. Rare earth permanent magnets for the green energy transition: Bottlenecks, current developments and cleaner production solutions. *Resour. Conserv. Recycl.* **2025**, *212*, 107966. [CrossRef]
4. Podmiljšak, B.; Saje, B.; Jenuš, P.; Tomše, T.; Kobe, S.; Žužek, K.; Šturm, S. The future of permanent-magnet-based electric motors: How will rare earths affect electrification? *Materials* **2024**, *17*, 848. [CrossRef] [PubMed]
5. Akhtar, N.; Geyer, B.; Schrum, C. Larger wind turbines as a solution to reduce environmental impacts. *Sci. Rep.* **2024**, *14*, 6608. [CrossRef] [PubMed]
6. Moustafa, A.M. A three decade review of environmentally friendly vehicles sustainable development research. *Sustain. Futures* **2025**, *9*, 100565. [CrossRef]
7. Heim, J.W., II; Vander Wal, R.L. NdFeB permanent magnet uses, projected growth rates and Nd plus Dy demands across end-use sectors through 2050: A Review. *Minerals* **2023**, *13*, 1274. [CrossRef]
8. Aoyama, Y.; Miyata, K.; Ohashi, K. Simulations and Experiments on Eddy Current in Nd–Fe–B Magnet. *IEEE Trans. Magn.* **2005**, *41*, 3790–3792. [CrossRef]
9. Toda, H.; Xia, Z.; Wang, J.; Atallah, K.; Howe, D. Rotor eddy-current loss in permanent magnet brushless machines. *IEEE Trans. Magn.* **2004**, *40*, 2104–2106. [CrossRef]
10. Yamazaki, K.; Shina, M.; Miwa, M.; Hagiwara, J. Investigation of Eddy Current Loss in Divided Nd–Fe–B Sintered Magnets for Synchronous Motors Due to Insulation Resistance and Frequency. *IEEE Trans. Magn.* **2008**, *44*, 4269–4272. [CrossRef]
11. Mirzaei, M. Eddy current analysis in permanent magnets using the variational method. *IEEE Trans. Magn.* **2023**, *59*, 6300811. [CrossRef]
12. Plait, A.; Dubas, F. Two-dimensional eddy-current losses model and experimental validation through thermal measurements. *IEEE Trans. Instrum. Meas.* **2023**, *72*, 6003607. [CrossRef]
13. Yáñez, D.G.; Fernandez, D.; Martínez, M.; Guerrero, J.M. Loss model of NdFeB magnets considering resistivity variations with magnetization state and temperature. In *Proceedings of the 2025 IEEE Energy Conversion Conference Congress and Exposition (ECCE), Philadelphia, PA, USA, 19–23 October 2025*; IEEE: New York, NY, USA, 2025; pp. 1–7.
14. Jung, J.W.; Lee, B.H.; Kim, K.S.; Kim, S.I. Interior permanent magnet synchronous motor design for eddy current loss reduction in permanent magnets to prevent irreversible demagnetization. *Energies* **2020**, *13*, 5082. [CrossRef]
15. Pan, B.; Tao, D.; Ge, B.; Wang, L.; Hou, P. Analysis of Eddy Current Loss of 120-kW High-Speed Permanent Magnet Synchronous Motor. *Machines* **2022**, *10*, 346. [CrossRef]
16. Han, Y.; Zhang, Q.; Liu, Y.; Chen, S.; Ma, Z.; Li, Y.; Sun, J. Advanced Temperature Prediction for Electric Motors: A Review from Physical Foundations to Physics-Informed Intelligence. *Machines* **2026**, *14*, 305. [CrossRef]
17. Herbst, J.F. $R_2Fe_{14}B$ materials: Intrinsic properties and technological aspects. *Rev. Mod. Phys.* **1991**, *63*, 819–898. [CrossRef]
18. Itakura, M.; Watanabe, N.; Nishida, M.; Daio, T.; Matsumura, S. Atomic-resolution X-ray energy-dispersive spectroscopy chemical mapping of substitutional Dy atoms in a high-coercivity neodymium magnet. *Jpn. J. App. Phys.* **2013**, *52*, 050201. [CrossRef]
19. Tang, X.; Li, J.; Sepehri-Amin, H.; Bolyachkin, A.; Martin-Cid, A.; Kobayashi, S.; Kotani, Y.; Suzuki, M.; Terasawa, T.; Gohda, Y.; et al. Unveiling the origin of the large coercivity in (Nd, Dy)-Fe-B sintered magnets. *NPG Asia Mater.* **2023**, *15*, 50. [CrossRef]
20. Wang, Z.; Sasaki, T.T.; Une, Y.; Ohkubo, T.; Hono, K. Substantial coercivity enhancement in Dy-free Nd–Fe–B sintered magnet by Dy grain boundary diffusion. *Acta Mater.* **2023**, *248*, 118774. [CrossRef]
21. Vasilenko, D.Y.; Shitov, A.V.; Popov, A.G.; Gaviko, V.S.; Bratushev, D.Y.; Podkorytov, K.I.; Golovnya, O.A. Magnetic hysteresis properties and microstructure of high-coercivity (Nd,Dy)–Fe–B magnets with Dy less than 10 wt % and low oxygen. *Phys. Met. Metallogr.* **2022**, *123*, 145–154. [CrossRef]
22. Durgun, A.; Ohmer, D.; Katter, M.; Thul, A.; Steentjes, S.; Sepehri-Amin, H.; Oliver, G.; Dirba, I. Toward maximum utilization of heavy rare earths in sintered Nd–Fe–B magnets by grain boundary diffusion source and application area optimization. *Adv. Eng. Mater.* **2025**, *27*, 2501145. [CrossRef]
23. Wan, F.; Zhang, Y.; Han, J.; Liu, S.; Liu, T.; Zhou, L.; Deng, Z. Coercivity enhancement in Dy-free Nd–Fe–B sintered magnets by using Pr-Cu alloy. *J. Appl. Phys.* **2014**, *115*, 203910. [CrossRef]
24. Saito, T.; Nozaki, S.; Sajima, Y.; Nishio-Hamane, D. Coercivity of Nd–Fe–B hot-deformed magnets produced by the spark plasma sintering method. *AIP Adv.* **2017**, *7*, 056205. [CrossRef]
25. Li, W.; Feng, Q.; Chen, C.; Zhang, X.; Fu, Z.; Hou, Y.; Huang, Y. Microstructure optimization and magnetic properties enhancement of hot pressed Nd–Fe–B magnets via grain boundary diffusion of NdCu powder. *J. Magn. Magn. Mater.* **2023**, *567*, 170325. [CrossRef]

26. Zhu, C.; Liu, X.; Kan, X.; Liu, Y.; Wang, L. Effect of Grain Boundary Diffusion Pr and Cu on Properties of Sintered Nd–Fe–B Permanent Magnet. *J. Supercond. Nov. Magn.* **2023**, *36*, 1977–1982. [CrossRef]
27. Sergeant, P.; Bossche, A.V. Segmentation of Magnets to Reduce Losses in Permanent-Magnet Synchronous Machines. *IEEE Trans. Magn.* **2008**, *44*, 4409–4412. [CrossRef]
28. Sirimanna, S.; Zhang, X.; Haran, K. Investigation of the impact of magnet segmentation on high frequency eddy current losses in an interior permanent magnet motor. In *Proceedings of the 2022 IEEE Energy Conversion Congress and Exposition (ECCE), Detroit, MI, USA, 9–13 October 2022*; IEEE: New York, NY, USA, 2022; pp. 1–7.
29. Kiryakin, A.A.; Shchetinin, E.V. Study of heating of high-speed rotor of powerful synchronous generator taking into account methods of reducing magnetic losses and heating of permanent magnets. In Proceedings of the 2025 International Ural Conference on Electrical Power Engineering (UralCon), Magnitogorsk, Russia, 25–28 September 2025; pp. 1–10.
30. Huang, W.Y.; Bettayeb, A.; Kaczmarek, R.; Vannier, J.C. Optimization of magnet segmentation for reduction of eddy-current losses in permanent magnet synchronous machine. *IEEE Trans. Energy Convers.* **2010**, *25*, 381–387. [CrossRef]
31. Wei Li, W.; Zheng, L.; Bi, W.; Li, Y.; Zhu, M.; Feng, H.; Zhou, D.; Guo, Z. Effect of CaF_2 addition on the microstructure and magnetic and electrical properties of sintered Nd–Fe–B magnets. *IEEE Trans. Magn.* **2014**, *50*, 1001504.
32. Wang, Z.; Chen, R.; Yin, W.; Yan, C.; Tang, X.; Jin, C.; Lee, D.; Yan, A. Enhanced electric resistivity of die-upset magnets by segmented NdF_3 addition. *IEEE Trans. Magn.* **2014**, *50*, 2104103. [CrossRef]
33. Kautsara, Z.H.; Sepehri-Amina, H.; Tang, X.; Kulesh, N.; Sasaki, T.T.; Ohkubo, T.; Hono, K. Heavy rare earth-free high resistivity and coercivity Nd–Fe–B hot-deformed magnet developed by Pr-Cu diffusion and CaF_2-LiF eutectic addition. *J. Alloys Compd.* **2025**, *1010*, 177738. [CrossRef]
34. Sawatzki, S.; Dirba, I.; Schultz, L.; Gutfleisch, O. Electrical and magnetic properties of hot-deformed Nd–Fe–B magnets with different DyF_3 additions. *J. Appl. Phys.* **2013**, *114*, 133902. [CrossRef]
35. Kautsar, Z.H.; Sepehri-Amin, H.; Tang, X.; Iguchi, R.; Uchida, K.; Ohkubo, T.; Hono, K. High-resistivity anisotropic hot-deformed Nd–Fe–B magnets prepared from DyF_3 electrophoretic deposited powders. *J. Alloys Compd.* **2023**, *942*, 168855. [CrossRef]
36. Kim, K.M.; Kim, J.Y.; Kwon, H.W.; Kim, D.H.; Lee, J.G.; Yu, J.H. High electrical resistivity Nd–Fe–B die-upset magnet doped with eutectic DyF_3–LiF salt mixture. *AIP Adv.* **2017**, *7*, 056232. [CrossRef]
37. Xia, X.; Wei, G.; Wu, L.; Du, Y.; Tang, X.; Ju, J.; Wu, H.; Chen, R.; Yin, W.; Yan, A. Effect of nano-Cu addition on the diffusion behaviors of Dy in hot- deformed Nd–Fe–B magnets. *J. Alloys Compd.* **2023**, *952*, 170014. [CrossRef]
38. Hu, Y.; Li, J.; Sun, S.; Zhong, S.; Yang, M.; Yu, X.; Rehman, S.U.; Yu, X. Simultaneously enhancing coercivity and remanence of hot-deformed Nd–Fe–B magnets by flake copper powder assisted DyF_3 interflake addition. *J. Rare Earths* **2024**, *42*, 1282–1288. [CrossRef]
39. Liu, Q.; Zhang, L.; Xu, F.; Dong, X.; Wu, J.; Komuro, M. Dysprosium nitride-modified sintered Nd–Fe–B magnets with increased coercivity and resistivity. *Jpn. J. Appl. Phys.* **2010**, *49*, 093001. [CrossRef]
40. Saito, T. Electrical resistivity and magnetic properties of Nd–Fe–B alloys produced by melt-spinning technique. *J. Alloys Compd.* **2010**, *505*, 23–28. [CrossRef]
41. Hou, R.; Zhang, Z.; He, J.; Gong, W.; Xu, Z.; Lin, A. Measuring of electrical resistivity on NdFeB magnets using the Van-der-Pauw (VDP) Method. In Proceedings of the 2018 Conference on Precision Electromagnetic Measurements (CPEM 2018), Paris, France, 8–13 July 2018; pp. 1–2.
42. Shokrollahi, H.; Janghorban, K. Soft magnetic composite materials (SMCs). *J. Mater. Proc. Technol.* **2007**, *189*, 1–12. [CrossRef]

Disclaimer/Publisher's Note: The statements, opinions and data contained in all publications are solely those of the individual author(s) and contributor(s) and not of MDPI and/or the editor(s). MDPI and/or the editor(s) disclaim responsibility for any injury to people or property resulting from any ideas, methods, instructions or products referred to in the content.